79-4019

# Kinetic Model for Aerosol Formation in Rocket Contrails

J. W. Meyer*
*Lockheed Palo Alto Research Laboratory, Palo Alto, Calif.*

**A kinetic condensation model is presented for rocket contrail formation. The formulation treats condensation of water and acid species as a heterogeneous process occurring on soluble or insoluble nuclei particles in the rocket exhaust. The modeling objective is the prediction of condensate aerosol number densities and sizes in contrails. Numerical model results are presented for a $HCl/H_2O$ exhausting rocket at several ambient conditions. It is found that plume condensate aerosol properties are affected by the loading and size distributions of the nuclei particles, especially at high altitudes.**

## Nomenclature

$C$ = condensate mass concentration
$D$ = molecular diffusion coefficient
$e$ = saturated vapor pressure
$h$ = Harned coefficient
$\Delta H$ = latent heat of vaporization or solution
$I$ = ionic strength of solution
$m$ = molality (moles solute/1000 g water)
$M_2$ = average acid molality of aerosol
$n$ = aerosol particle concentration
$P$ = pressure
$P_1, P_2$ = partial pressures
$R, z$ = radial and axial plume coordinates
$r$ = aerosol particle radius
$\bar{r}$ = mode aerosol drop radius
$R$ = universal gas constant
$\bar{S}_1$ = mode drop $H_2O$ saturation ratio
$\bar{S}_2$ = mode drop acid saturation ratio
$t$ = time
$T$ = temperature
$u, v$ = axial and radial plume velocity components
$W$ = molecular weight
$W_\ell$ = aerosol liquid concentration per unit volume
$X_e$ = local mass fraction of exhaust products in plume
$Y$ = mass fraction of condensible species
$Z$ = valence
$\alpha$ = thermal accommodation coefficient
$\beta$ = vapor molecule condensation coefficient (sticking coefficient)
$\kappa$ = plume thermal conductivity
$\delta$ = nuclei particle diameter
$\lambda$ = mean free path
$\sigma$ = liquid surface tension
$\gamma$ = activity coefficients
$\mu$ = mass of condensate in drop
$\theta$ = excess temperature of drops over surroundings
$\rho$ = density
$\Psi$ = pseudostream function
$\omega$ = number of aerosol particles/g exhaust products

*Subscripts*

1 = water
2 = second condensible component in plume (e.g., HCl)
3 = soluble nuclei material component in solution
$e$ = exhaust properties
$i$ = aerosol drop class distinguished by size and type of nuclei particle
$d$ = drops

*Superscripts*

$\infty$ = properties over a plane surface

Received Dec. 18, 1977; revision received Sept. 1, 1978. 

Index categories: Jets, Wakes, and Viscid-Inviscid Flow Interactions; Multiphase Flows.

*Research Scientist, Fluid Mechanics Laboratory. Member AIAA.

## Introduction

COMBUSTION of ammonium perchlorate containing solid rocket propellants yields HCl in the exhaust products. Formation of rocket contrails is aided by the hygroscopic effect of the HCl, and acid aerosol trails may form under much warmer and drier conditions than needed for normal aircraft contrails to exist. Detailed knowledge of condensate aerosol size distributions and number densities in rocket contrails is of interest both for visibility and detection considerations, and with regard to environmental effects of acid rainout from large rocket booster ground clouds. The main impetus of this work has been rocket plume visibility questions.

In the present paper, a predictive numerical model is described for condensation in atmospheric plumes. Condensation of two vapor species (water and a second condensible component) is modeled as a kinetic process of aerosol droplet growth on pre-existing solid nuclei particles in the plume, i.e., heterogeneous condensation. In the model formulation, the nuclei may be either insoluble primary smoke particles, such as metal oxides or carbon, or they may be soluble materials, such as salts, which have additional hygroscopic effects. Model results are presented illustrating the condensation processes in an $H_2O/HCl$ containing plume under several combinations of ambient conditions and nuclei particle loadings.

A computer program representing the present condensation model constitutes the basis for one portion of an operational rocket plume visibility computer code.[1] Three main submodels are used in the makeup of the complete code: an afterburning turbulent jet flowfield model, a condensation model, and a background and target visibility model. Only the condensation model is described in detail in this paper, the other submodels are treated elsewhere.[2,3]

Most previously published work in the area of predicting aircraft[4-6] and rocket[7,8] contrails has taken an equilibrium rather than a kinetic condensation approach. Under many conditions, an equilibrium treatment should yield reasonably valid results as to the total mass concentration of condensate (i.e., $g/M^3$) formed in the plume. However, it cannot say anything about the size of the aerosol particles which is of major importance with regard to light scattering and visibility. Generally, kinetic treatments of condensation in gasdynamic flows such as wind tunnel nozzles are based on

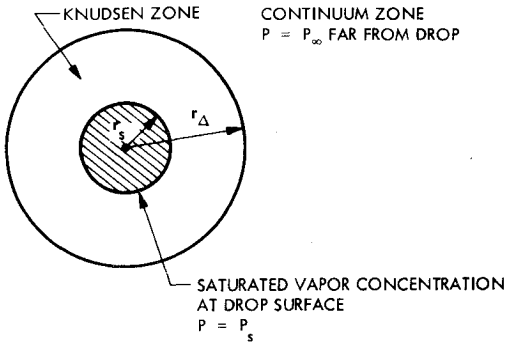


**Fig. 1 Vapor field zone surrounding condensing droplet.**

homogeneous, as opposed to heterogeneous, condensation.[9] The present treatment is most closely akin to the so-called microphysical meteorological models for prediction of cloud formation and rainfall.[10,11] Atmospheric condensation is invariably a heterogeneous nucleation process, usually on soluble (NaCl) nuclei particles. Sophisticated models of this type have been described in the meteorological literature.[12-14]

Currently some other workers are also taking a heterogeneous nucleation, kinetic approach to the analysis of the plume condensation problem. Miller[15-18] has discussed plume condensation in general terms in several papers and has also presented examples of calculated droplet growth behavior on plume streamlines. These calculations were uncoupled in terms of heat and mass exchange between phases, e.g., the condensibles are not subtracted from the vapor phase as condensation progresses. Victor[19] has also described a kinetic model for droplet growth in plumes and in smoke chambers. Victor's model contains mass and energy balances, but makes other restrictive approximations such as treating just the water component kinetically and using a local equilibrium assumption to determine droplet acid content. Other differences between the preceding models and the condensation model presented in this paper include variations between the actual single droplet mass transfer equations, somewhat different nucleation scenarios, an alternate method for solution properties calculations, and a different approach to defining the particle paths along which the condensation occurs.

## Turbulent Jet Flowfield

The rocket plume flowfield in which condensation takes place is modeled as an axisymmetric, turbulent freejet. The flowfield model is described in detail by Thomas[2] and will not be discussed further here. The present condensation model calculations are, for the most part, decoupled from the flowfield calculations. Fundamentally, the degree of condensate formation is assumed not to have an impact on the overall dynamics of the jet flow. Therefore, the exhaust products/air-mixing ratio and enthalpy at any point in the plume remain the same either with or without condensation. This assumption is well justified considering the rather small changes in plume density and temperature likely to be induced by condensation. As a consequence of this assumption, the flowfield and condensation computations can be run sequentially. However, during the condensation computations, proper account may still be taken of heat and mass exchange between vapor and condensate phases.

A more serious fundamental approximation utilized in the modeling is that all plume nuclei and condensate particles are assumed to follow average exhaust particle paths established by the turbulent diffusion flowfield calculation. Specifically, condensation calculations are carried out along plume lines characterized by a constant pseudostream function parameter, $\Psi$, where

$$\Psi(R,z) = \int_0^R X_e \rho u R \mathrm{d}R \Big/ \int_0^\infty X_e \rho u R \mathrm{d}R \tag{1}$$

Here $X_e$ is the local mass fraction of exhaust products in the plume. Under this basic assumption, plume particles stay on well-defined trajectories; thus, condensate drops can always be identified with their original nuclei and tracked. The implicit assumption that the spreading of the particles and exhaust gases are identical is a good one, since these particles are in the micron size range, or smaller, and are well able to follow the gas motions. On the other hand, diffusion of drops formed on a particular $\Psi$ path to other parts of the plume is not accounted for under this formulation.

Unfortunately, the more completely correct treatment is not feasible computationally. This would essentially entail writing a Fickian diffusion type of conservation equation for each distinguishable condensate drop class,

$$\rho u \frac{\partial n_j}{\partial Z} + \rho v \frac{\partial n_j}{\partial R} = \frac{D_T}{R} \frac{\partial}{\partial R}\left[R \frac{\partial n_j}{\partial R}\right] + S \tag{2}$$

where $n_j$ is the number density of drops in class $j$, $D_T$ is the turbulent diffusion coefficient, and $S$ represents condensation rate terms. A drop class $j$ is characterized by three parameters which distinguish individual drops and influence their growth rates: the drop radius, the acid strength or molality of the drop, and the amount of nuclei material contained in the drop. In order to make a computer calculation, one would have to distribute the plume drops into a number of finite bins, each representing some range of values of these three parameters. Drops are then shuffled between bins as they grow, dilute, and so forth. All drops in each bin would constitute a drop class obeying Eq. (2). The computational problem is that even for very coarse increments in bin properties, the number of bins and, therefore, the number of coupled equations that must be solved is intractable. For example, if we chose a bin set characterized by 10 drop sizes, 10 different acid molalities, and 10 nuclei sizes, one already has $10^3$ total distinguishable bins and $10^3$ coupled equations to integrate. The reader may be familiar with the chemically reacting plume computational models wherein individual chemical species are diffused. This condensation problem example is analogous to solving the reacting plume problem with $10^3$ chemical species.

## Heterogeneous Condensation Model

### Droplet Growth Equations

The basic droplet growth equations to be integrated along plume particle pathlines are of the form:

$$\frac{\mathrm{d}u_{1i}}{\mathrm{d}t} = \frac{4\pi r_i^2}{RT} \frac{D_1 W_1 (P_1 - e_{1i})}{\left[\frac{D_1}{\beta_1}\left(\frac{2\pi W_1}{RT}\right)^{1/2} + \frac{r_i}{1 + (\lambda_i / r_i)}\right]} \tag{3}$$

$$\frac{\mathrm{d}\mu_{2i}}{\mathrm{d}t} = \frac{4\pi r_i^2}{RT} \frac{D_2 W_2 (P_2 - e_{2i})}{\left[\frac{D_2}{\beta_2}\left(\frac{2\pi W_2}{RT}\right)^{1/2} + \frac{r_i}{1 + (\lambda_i / r_i)}\right]} \tag{4}$$

where $\mu_{1i}$ and $\mu_{2i}$ are the masses of water and acid contained in the $i$th drop. The index $i$ distinguishes the drops as they are tracked and refers initially to the size and type of nuclei on which the drops have grown.

Equations (3) and (4) characterize the mass addition rate from the vapor to a motionless drop in both the continuum and the free molecular flow regimes. The growth equation development is based on Fukuta[20] and proceeds as follows: Conceptually, the vapor field surrounding a droplet is divided into two zones—a free molecular flow or "Knudsen" zone extending out to one mean free path from the drop surface, and a continuum zone beyond, as illustrated by Fig. 1. The

rate that diffusing vapor arrives at the zone interface is given by the classical quasisteady continuum expression

$$\left.\frac{d\mu}{dt}\right|_c = 4\pi r_\Delta \frac{DW}{RT}(P_\infty - P_\Delta) \tag{5}$$

The free molecular flow expression for the rate of vapor deposition on the drop surface is:

$$\left.\frac{d\mu}{dt}\right|_K = 4\pi r_s^2 \left(\frac{W}{2\pi RT}\right)^{1/2} \beta (P_\Delta - P_s) \tag{6}$$

where $\beta$ is the condensation coefficient (the fraction of molecules striking the surface which condense), $P$ is condensible vapor partial pressure, $\Delta$ signifies the zone interface, $S$ the drop surface, and $\infty$ far from the drop, as shown in Fig. 1.

Under the quasisteady approximation, the rates given by Eqs. (5) and (6) must be equal. Therefore, combining Eqs. (5) and (6), one obtains, with some rearrangement, the following expression:

$$P_\infty - P_\Delta = \frac{r_s^2 \beta}{r_\Delta D}\left(\frac{RT}{2\pi W}\right)^{1/2} \frac{P_\infty - P_s}{\left[1 + \frac{r_s^2 \beta}{r_\Delta D}\left(\frac{RT}{2\pi W}\right)^{1/2}\right]} \tag{7}$$

The substitution of Eq. (7) back into Eq. (5), using the assumption that $r_\Delta = r_s + \lambda$, yields a growth equation in the form of Eqs. (3) and (4).

Saturated vapor pressures at the drop surfaces to be used in Eqs. (3) and (4) are functions of the drop radius as given by the classical Kelvin equation[21]:

$$e_{1i} = e_{1i}^\infty \exp(2W_1\sigma_i/\rho_i RT_i r_i) \tag{8}$$

$$e_{2i} = e_{2i}^\infty \exp(2W_2\sigma_i/\rho_i RT_i r_i) \tag{9}$$

Here $e_{1i}^\infty$ and $e_{2i}^\infty$ are the saturated vapor pressures of water and acid over plane solution surfaces of the same composition as the drop. The approach for calculating mixed solution saturated vapor pressures is described later.

It should be noted that the droplet growth model treats only condensation. Agglomeration phenomena, such as that caused by Brownian motion or turbulent mechanisms, are not included. Also, no attempt is made to account for convective transport to the drops due to particle slip in the turbulent field. The assumption is made that all these factors are negligible under plume conditions due to the small size of the drops, the relatively low number densities and rapid dilution rates, and the comparatively short time frame of interest. These assumptions can all be rather easily supported by order-of-magnitude calculations. For example, neglecting convective mass transfer to the drops is justified by the fact that condensation cannot occur until the hot exhaust gases have undergone considerable cooling by air dilution; typically the dilution factor is $10^2$ or more. This means that local mean velocities and turbulent velocity fluctuations are quite low in the condensation zone and droplet velocity lags should be minimal. However, even assuming an extreme case of a 1 $\mu$ drop with a slip velocity of $10^2$ m/s, standard convective correlations[22] predict only a 10% enhancement of the mass transfer in comparison to Eqs. (3) and (4). In typical cases the correction would be only a small fraction of this amount.

The coefficients $\beta_1$ and $\beta_2$ appearing in Eqs. (3) and (4) are important parameters since the condensation rate is proportional to $\beta$ for small drop sizes. Most meterological modelers use the classic value for water measured by Alty and MacKay[23] of $\beta_1 = 0.036$, often rounded off to 0.04. Fukuta and Walter[20] have summarized condensation coefficient data for water and ice from eleven investigators and, in the temperature range of interest here, most confirm this low value of sticking probability. However, Miller[15] has pointed out that recent measurements of the condensation coefficient, such as by Mills and Seban,[24] have given much higher values and that they question the accuracy of earlier work. At present, there still appears to be more evidence for low $\beta$ values, but this is at least controversial. In addition, it is uncertain if pure water values can be applied to strong acid solutions and, finally, there are no data available for the condensation coefficient of the acid molecules. The best values are, therefore, quite uncertain.

In the present calculations, low values ($\beta_1 = \beta_2 = 0.04$) of the condensation coefficients are used for the most part, but selected cases are repeated with $\beta_1 = \beta_2 = 1$ in order to investigate the sensitivity of the results to these parameters.

#### Drop Temperatures

During the condensation process, individual drop temperatures are raised slightly with respect to the surroundings because of the necessity of conducting away latent heat released at the drop's surface. A quasisteady droplet heat balance similar to the mass balance discussed previously yields the following expression for the $i$th drops excess temperature:

$$\theta_i = \left[\Delta H_1 \frac{d\mu_{1i}}{dt} + \Delta H_2 \frac{d\mu_{2i}}{dt}\right]\left[\frac{\alpha P(5/2)R}{(2\pi WRT)^{1/2}} + \frac{\kappa}{r_i[1 + (\lambda/r_i)]}\right] \Bigg/ \left[\frac{4r_i^2 \alpha P(5/2) R\kappa}{(2\pi WRT)^{1/2} r_i[1 + (\lambda/r_i)]}\right] \tag{10}$$

Individual drop temperatures based on this expression are tracked and used in the drop vapor pressure computations. A thermal accommodation coefficient ($\alpha$) of unity is agreed to by most investigators and this value is used in the present studies. In numerical calculations, the drop excess temperatures are normally found to be small ($<1$K) when low condensation coefficient values are used.

#### Nucleation

The condensation model is formulated to consider up to 270 distinguishable condensation nuclei sizes and types. These are divided into six general types: 1) insoluble primary rocket smoke particles, 2) soluble primary smoke particles, 3) a second chemical type of soluble primary smoke particles, 4) insoluble primary smoke particles with a thin soluble coating, 5) soluble ambient nuclei particles (NaCl), and 6) insoluble ambient nuclei particles.

Size distributions containing a maximum of 45 discrete radii for each nuclei type are utilized in the model. The discrete distributions are generated from parameterized distributions of the form:

$$\frac{dN}{d\delta} = a_1 \delta^{q_1} \exp(-b_1 \delta^{s_1}) + a_2 \delta^{q_2} \exp(-b_2 \delta^{s_2}) \tag{11}$$

where $N$ is the number of nuclei normalized by the total number of nuclei, $\delta$ is the nuclei diameter in $\mu$, and $a_1, q_1, b_1, s_1, a_2, q_2, b_2, s_2$ are distribution shape parameters. Given the mass fraction of each type of nuclei solids in the rocket exhaust, $Y_{ei}$, and the size distribution function, one may calculate numbers of nuclei in each discrete size bin per unit mass of rocket exhaust products as follows:

$$\omega_i \equiv \frac{n_{ie}}{\rho_e} = \frac{Y_{ei}\int_{\delta_{i-1}}^{\delta_i} \frac{dN}{d\delta} d\delta}{\int_{\delta_{\min}}^{\delta_{\max}} \rho_n \frac{\pi}{6}\delta^3 \frac{dN}{d\delta} d\delta} \tag{12}$$

where $\delta_{i-1}$, $\delta_i$ define the particle diameter limits of the size bin, $\delta_{\min}$ and $\delta_{\max}$ are the overall range of nuclei sizes considered, and $\rho_n$ is the density of the solid nuclear material.

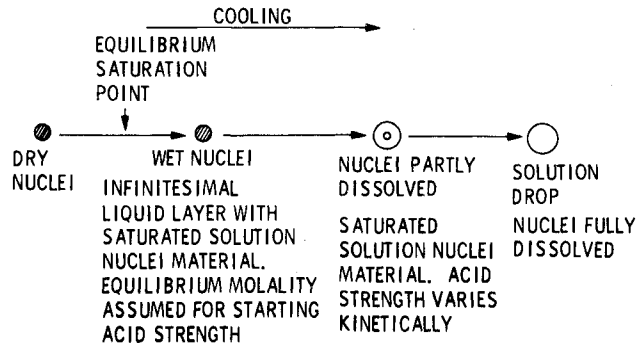


**Fig. 2 Droplet growth stage model for soluble nuclei.**

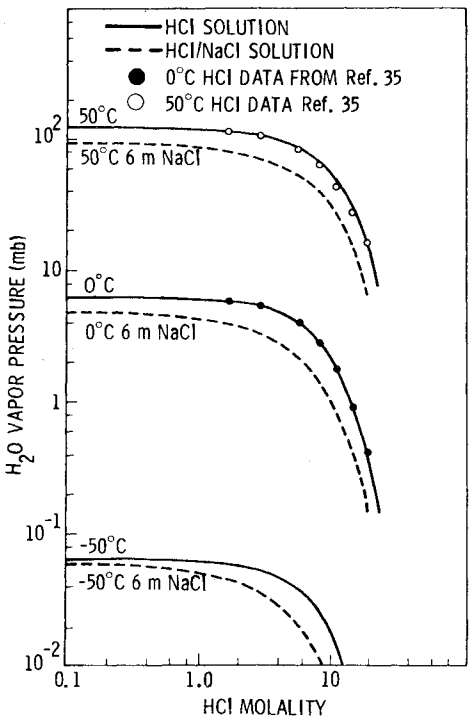


**Fig. 3 $H_2O$ saturated vapor pressures over HCl and HCl/NaCl solutions.**

The number density of nuclei at any point in the plume can then be computed simply from the overall dilution (i.e., $X_e$).

$$n_l = \omega_i \rho X_e \tag{13}$$

Any ambient nuclei are inserted at the plume saturation points and then are diluted in the same manner as the rocket smoke particles. This handling of ambient particles is a crude approximation, but ambient nuclei are expected to be important only on exceedingly rare occasions. Even nonaluminized propellants typically contain on the order of 1% metals or metal compounds as ballistic modifiers. The corresponding quantity of metal oxide primary smoke produced in combustion easily overwhelms foreseeable ambient particulates, even under hazy conditions at ground level.

In performing the condensation calculations, the saturation point is first located on each plume pathline using an equilibrium condensation algorithm. Kinetic calculations [i.e., integration of Eqs. (3) and (4)], are begun at this point. For the purpose of starting the calculation, the nuclei are assumed to be initially soaked with an infinitesimal liquid layer of the same acid strength as determined in the equilibrium calculation. Figure 2 illustrates the nucleation and growth stage model used for soluble nuclei particles. In the case of insoluble nuclei, once some nuclei have started to grow

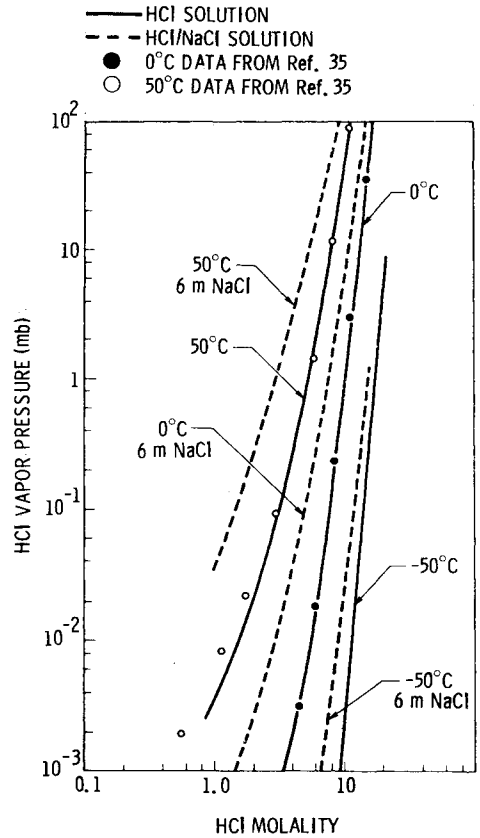


**Fig. 4 HCl saturated vapor pressures over HCl and HCl/NaCl solutions.**

drops and their acid molalities are determined kinetically, the remaining smaller and, as yet unactivated, nuclei are assigned starting acid strengths equal to the average of the growing drops. In early calculations a somewhat different procedure was used in which starting strengths were based on an equilibrium calculation which considered just the quantities of condensibles left in the vapor phase. However, it was found that this generally led to drops being born with molalities somewhat different from their previously activated fellows, but then adjusting to close to that of the other drops in just a brief time period. This happens because the water and acid are generally out of equilibrium to different extents (i.e., $s_1 \neq s_2$) during the activation and early growth phase and thus the equilibrium and kinetic molalities differ. Typically, model calculations show very little variation of molality across the spectrum of drop sizes; therefore, it was decided to assign average acid strengths at activation and avoid the physically unrealistic molality adjustment. The equilibrium approach is still used in the case of soluble nuclei, since the acid molality then does tend to vary with drop size due to the different concentrations of nuclei material.

To avoid starting problems near $\mu_{1i} + \mu_{2i} = 0$, Eqs. (3) and (4) are not integrated simultaneously until the liquid layer on each nuclei particle has grown to a specified small but finite size—typically 10% of the nuclei volume. Instead, only Eq. (3) is integrated initially to determine $\mu_{li}$ and the acid content is calculated by assuming the molality remains at an equilibrium value during this brief starting phase.

#### Interphase Heat and Mass Balances

Masses of water and acid in individual liquid drops are calculated by integrating Eqs. (3) and (4) along the $\Psi$ pathlines in the plume. Total plume liquid concentration is obtained by summing the individual masses over all drops.

$$C_1 = \sum_i n_i \mu_{1i}, \quad C_2 = \sum_i n_i \mu_{2i} \tag{14}$$

Then the mass fractions of condensibles remaining in the vapor phase simply are:

$$Y_{v1} = Y_1 - C_1/\rho, \quad Y_{v2} = Y_2 - C_2/\rho \tag{15}$$

where $Y_1$ and $Y_2$ are the total water and acid mass fractions from the jet flowfield calculation.

Plume temperatures are slightly perturbed from the original flowfield values due to latent heat release. The local plume temperature, corrected for the latent heat effect, is given by:

$$T = T_0 + \frac{1}{C_p}\left\{\frac{C_1}{\rho}\Delta H_1 + \frac{C_2}{\rho}\Delta H_2\right\} \tag{16}$$

where $T_0$ is the plume temperature determined in the non-condensing computation.

#### Saturated Vapor Pressure in Mixed Solutions

Water- and acid-saturated vapor pressures, $e_{1i}^{\infty}$ and $e_{2i}^{\infty}$ in Eqs. (8) and (9), are functions of three variables in the general case of soluble condensation nuclei. These variables are the drop temperature, the drop's acid molality $m_{2i}$, and the drop's salt molality $m_{3i}$. Here "salt" is used as a generic term for any soluble nuclei material. The procedure used in the vapor pressure calculations is based on activity coefficients and osmotic coefficients. The model is constructed to handle mixed solutions of multivalent electrolytes consisting of one acid and one salt.

The basic solution properties data input for the vapor pressure calculations are tables, with molality as the independent variable, of STP values of the pure solution mean ionic activity coefficient, $\gamma$ (25°C), the osmotic coefficient, $\phi$ (25°C), the relative partial molal enthalpy, $\bar{L}_2$ (25°C), and the relative partial molal heat capacity $\bar{J}_2$ (25°C). Compilations of the $\gamma$ and $\phi$ data are widely available in the literature.[25-28] The other parameters ($\bar{L}_2$ and $\bar{J}_2$) are used to compute $\gamma$ and $\phi$ values at nonstandard temperatures. These data are more difficult to come by, but good data are available for HCl.[29]

Activity coefficients and osmotic coefficients of the pure solutions at a general temperature are calculated from the STP data using an extrapolation method from Harned.[28] Then, mixed acid/salt solution properties are derived from Harned's rule which relates mixed solution properties to pure solution data through empirical Harned coefficients. This rule states that[30]

$$\log_{10}\gamma_2 = \log_{10}\gamma_{2(0)} - h_{23}I_3, \quad \log_{10}\gamma_3 = \log_{10}\gamma_{3(0)} - h_{32}I_2$$

$$I = I_2 + I_3 \tag{17}$$

where

$\gamma_2$ = activity coefficient of acid in mixed solution
$\gamma_3$ = activity coefficient of salt in mixed solution
$I_2, I_3$ = ionic strength of acid and salt in solution
$\gamma_{2(0)}$ = activity coefficient of acid in pure acid solution of ionic strength $I$
$\gamma_{3(0)}$ = activity coefficient of salt in pure salt solution of ionic strength $I$
$h$ = empirical Harned coefficients

The ionic strength $I$ is defined as:

$$I = \sum_j \frac{m\nu_j}{2} Z_j^2 \tag{18}$$

where $m$ is the solute molality, $\nu_j$ is the number of positive or negative ions per solute molecule, and $Z_j$ is the ion valence. Note that for a 1:1 electrolyte, such as HCl, $I$ is equal to the HCl molality.

The Harned coefficients are functions of the particular solute pair and, in addition, generally of the total ionic strength and temperature of the mixed solution. Fortunately, the latter variations appear to be fairly weak. Adequate Harned coefficient data are available for HCl with a number of salts.[30-34] However, no literature data have been found for mixed solutions containing *HF*, which is the other major acid component likely to be found in rocket exhaust products.

Through the use of the Harned coefficient approach mixed solution activity coefficients, osmotic coefficients, and ultimately solvent and solute vapor pressures can be calculated from pure solution data. The detailed expressions for these computations, as used in the present model, are omitted here for brevity but may be found in Ref. 1. Saturated vapor pressures calculated using this method are shown in Figs. 3 and 4 for both HCl and HCl/NaCl mixed solutions. Water saturated vapor pressures as a function of HCl molality are given in Fig. 3 and HCl pressures are given in Fig. 4. Above 0°C, direct vapor pressure data are available for HCl solutions[35]; these data are also included for comparison and show good agreement.

It should be pointed out that solution properties are basically empirical and little data are available for temperatures below 0°C. Lower temperature properties are essentially extrapolated. The extrapolation method is based on thermodynamic relations,[28] but is still rather long to reach high altitude temperatures. It would be desirable to obtain low-temperature solution vapor pressure data, particularly for the volatile solute, in order to validate the present approach at low temperatures.

#### Freezing Model

Liquid freezing points, as well as $H_2O$ vapor pressures, are highly depressed by the presence of acid solutes in the aerosol droplets. For example, the HCl azeotropic mixture, about 9 molal, freezes at −78°C. In the present treatment, a freezing analysis is used which assumes only pure water ice can constitute the solid phase formed in solution drops. The equilibrium freezing temperature, $T_f$, is calculated from the requirement that the freezing point is a triple point where

$$e_{1i}^{\infty}(\text{solution drop}) = e_{1i}^{\infty}(\text{ice}) \tag{19}$$

This approach allows the handling of quite general solutes, but does not, of course, take into consideration the possible formation of complex acid/water solid phases. Drop-freezing temperatures are calculated in the model at each integration step. In general, condensation nuclei are not necessarily efficient freezing nucleation sites.[11] Therefore, the possibility of supercooling is allowed for, and supercooling temperatures, $\Delta T_s$, are assigned for each type of nuclei substance. In the model calculations, if and when the drop temperatures fall below $T_f - \Delta T_s$, the drops are treated as water ice during subsequent growth or evaporation. The acidity of the frozen drops is not tracked beyond the freezing point, and the latent heat of freezing is neglected for computational convenience.

#### Numerical Integration Method

When both acid and water condensibles are present, the droplet growth equations are moderately stiff. As one approaches an equilibrium situation [$P_1 = e_{1i}$ and $P_2 = e_{2i}$ in Eqs. (3) and (4)] small changes in drop molality can produce large relative changes in the condensation rates. Early model results, using a fully explicit integration scheme, generally showed oscillations in droplet molality developing as the kinetic solution approached equilibrium.

To avoid this problem, a Crank-Nicholson implicit method with local linearization is used for differencing the water and acid content in each class of drops. Under this differencing scheme, the forward values of water and acid mass in the $i$th drop are given by the formulae:

$$\mu_{1i}^{n+1} = \mu_{1i}^{n} + \frac{\Delta t\left[\mathring{\mu}_{1i}^{n}\left(1 - J_{22}\frac{\Delta t}{2}\right) + \mathring{\mu}_{2i}^{n}\frac{\Delta t}{2}J_{12}\right]}{1 - (J_{11} + J_{22})\frac{\Delta t}{2} + (J_{11}J_{22} - J_{21}J_{12})\frac{\Delta t^2}{4}} \tag{20}$$

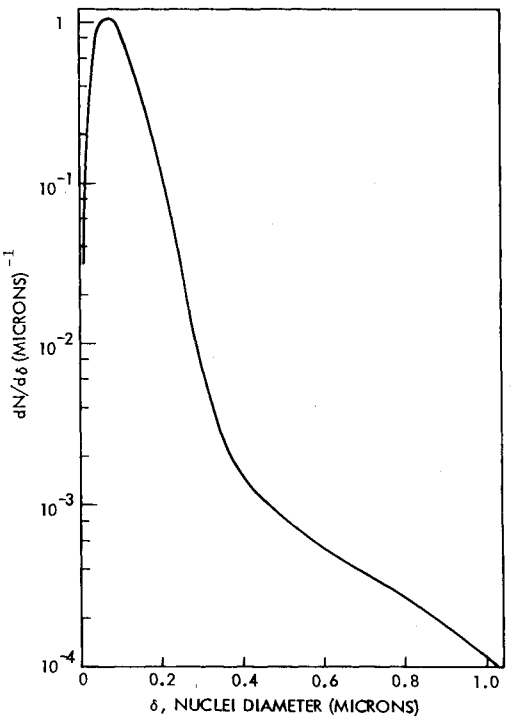


**Fig. 5 Size distribution function for $Al_2O_3$ rocket primary smoke particles Eq. (11) parameters: $a_1 = 5.6 \times 10^4$, $p_1 = 3$, $b_1 = 41.27$, $n_1 = 1$, $a_2 = 5.6$, $p_2 = 2$, $b_2 = 10.5$, $n_2 = 0.5$.**

$$\mu_{2i}^{\eta+1} = \mu_{2i}^{\eta} + \frac{\Delta t\left[\mathring{\mu}_{1i}^{\eta}\frac{\Delta t}{2}J_{21} + \mathring{\mu}_{2i}^{\eta}\left(1 - J_{11}\frac{\Delta t}{2}\right)\right]}{1 - (J_{11}+J_{22})\frac{\Delta t}{2} + (J_{11}J_{22} - J_{21}J_{12})\frac{\Delta t^2}{4}} \quad (21)$$

where

$$\mathring{\mu}_{1i} \equiv \left(\frac{\partial \mu_1}{\partial t}\right)_i \qquad \mathring{\mu}_{2i} \equiv \left(\frac{\partial \mu_2}{\partial t}\right)_i$$

$$J_{11} = \left(\frac{\partial \mathring{\mu}_1}{\partial \mu_1}\right)_{i,\mu_2} \qquad J_{12} = \left(\frac{\partial \mathring{\mu}_1}{\partial \mu_2}\right)_{i,\mu_1}$$

$$J_{21} = \left(\frac{\partial \mathring{\mu}_2}{\partial \mu_1}\right)_{i,\mu_2} \qquad J_{22} = \left(\frac{\partial \mathring{\mu}_2}{\partial \mu_2}\right)_{i,\mu_1}$$

The Jacobean terms $(J_{11}, J_{12}, J_{21}, J_{22})$ are evaluated numerically by perturbing the drop masses $\mu_{1i}$ and $\mu_{2i}$.

The implicit integration approach has eliminated problems associated with equation system stiffness.

## Condensation Model Results for $H_2O$/HCl

In this section condensation model results are presented which illustrate the rocket plume condensation processes under a number of different conditions. A slightly off-axis ($\Psi = 0.167$) streamline is considered in each case. The condensibles are assumed to be $H_2O$ and HCl with $\beta_1 = \beta_2 = 0.04$, except where noted. Rocket parameters, such as size, flight velocity, exhaust composition (20% $H_2O$, 20% HCl), and exhaust temperature, were arbitrarily selected and are not representative of any particular air-launched missile. Rocket parameters are invariant in all cases with the single exception of the type and loading of nuclei material (primary smoke) assumed to be present in the exhaust. Calculations are performed for both a moderate loading (5%), and much lower loading (0.05%), of primary smoke in order to reveal the effects of nuclei content on the condensate aerosol.

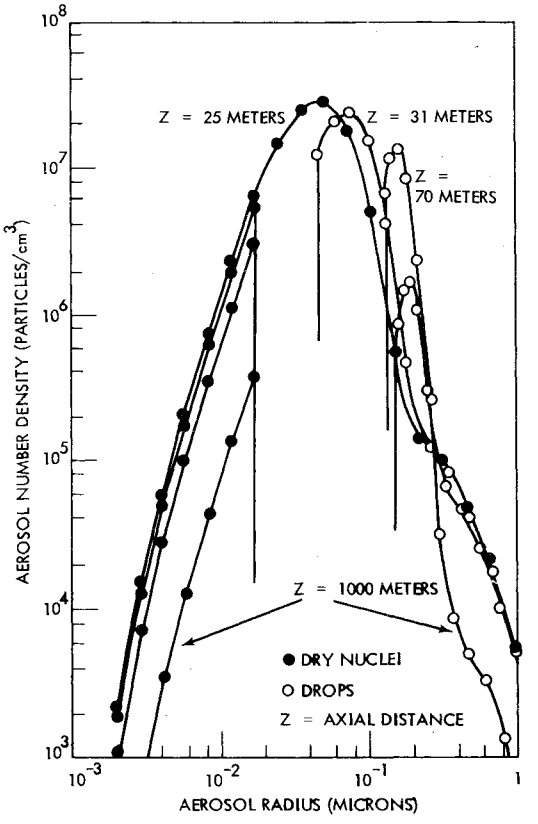


**Fig. 6 Growth of condensate aerosol spectrum in a rocket contrail, exhaust nuclei solids mass fraction = 0.05, altitude 7 km.**

Size data on primary smoke particles from rocket motors are rather inadequate for our purposes. Recent studies have been conducted by Dawbarn.[36] Most particle sampling work has been motivated by particle-related performance losses and has concentrated on determining the mass mean diameter. Small particles, though numerous, contribute little to the total mass and the primary smoke arithmetic mean diameter might easily be an order of magnitude smaller than the mass mean diameter. In our case, total numbers of particles which may act as nuclei are the key factor; sizes as small as $10^{-3} - 10^{-2}\ \mu$ can be important. Using the existing rocket particle data, which are likely to be biased toward larger particles, could greatly underestimate the number of available nuclei.

In these calculations a size distribution recommended by Dawbarn[37] (shown in Fig. 5) is used for $Al_2O_3$ primary smoke. This distribution was obtained by analysis of samples collected from a very large, in-flight, motor plume about 10 min after firing. The data extend to lower sizes than that from earlier studies. Of course, primary smoke properties of particle size and chemical composition would normally vary with propellant and motor configurations. This $Al_2O_3$ distribution is adequate for the present purpose of illustrating the operation of the model, but should not be taken to apply to primary smoke in any general sense.

### Results at 7 km Altitude

The first set of results is computed assuming ambient conditions are the standard atmosphere at 7 km altitude (243 K, 411 mb), and a relative humidity of 40% (over ice). Primary smoke is taken to be insoluble $Al_2O_3$ particles and to represent 5% of the rocket effluent by weight. Twenty discrete nuclei radii ranging from 0.002-2 $\mu$ are used to represent the possible range of nuclei. Number densities in each size class are based on the Fig. 5 distribution function.

Figure 6 illustrates the aerosol spectrum grown on the nuclei at four plume stations at distances of 25, 31, 70, and 1000 m behind the rocket. In this case, saturation conditions were reached just past the 25-m position, so the first curve

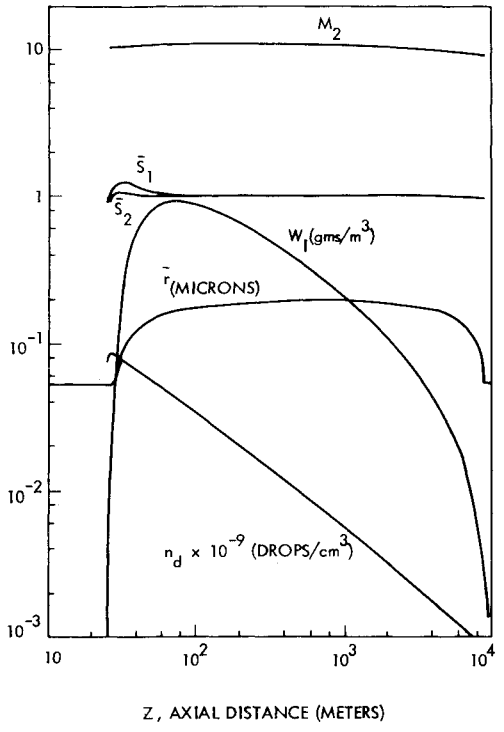


**Fig. 7 Rocket plume condensate aerosol parameters, exhaust nuclei solids mass fraction = 0.05, altitude 7 km.**

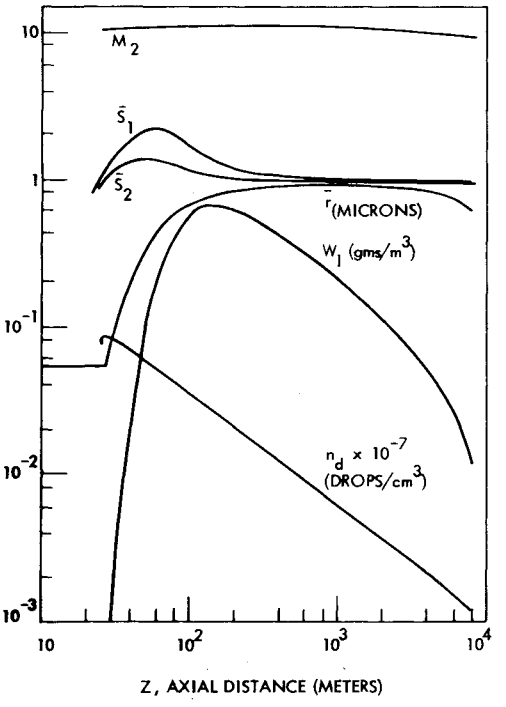


**Fig. 8 Rocket plume condensate aerosol parameters, exhaust nuclei solids mass fraction = 0.0005, altitude 7 km.**

represents the dry nuclei distribution only. Once saturation occurs, rapid droplet growth is started and, as can be seen in the illustration, all nuclei down to 0.025 $\mu$ in size are activated. Due to greater surface area/volume ratios, smaller drops grow much faster relative to larger ones and, characteristically, a broad range of nuclei eventually grow into a rather narrow spectrum of drop sizes. In this case, 99% of the drops have radii between 0.17 and 0.25 $\mu$ at the 1000-m position.

Other condensation parameters for the 7 km, 5% primary smoke example are plotted in Fig. 7 as a function of axial distance. These parameters include the average HCl molality of the aerosol $M_2$, the total condensate concentration $W_l$ in g/m$^3$, the drop number density $n_d$, the mode drop radius $\bar{r}$, and the water and HCl saturation ratios $\bar{S}_1$ and $\bar{S}_2$ over the mode drop where $S_{1i} \equiv P_1/e_{1i}$, $S_{2i} \equiv P_2/e_{2i}$. The contrail formed is nonpersistent and was almost completely evaporated at the point where the calculations were stopped. The aerosol drops are strongly acid and remain so throughout the life of the contrail. The condensate concentration peaks at the 75-m position and thereafter decays due to dilution and, ultimately, to evaporation. Saturation ratios only briefly reach values of $\bar{S}_1 = 1.3$ and $\bar{S}_2 = 1.1$ before the supersaturation collapses; a near-equilibrium state, where $\bar{S}_1$ and $\bar{S}_2$ differ only very slightly from unity, is maintained over most of the contrail's life. None of the drops freeze due to their high HCl concentrations.

In the second example, the previous calculations are repeated with the numbers of available condensation nuclei reduced by a factor of 100, i.e., with an exhaust primary smoke loading of only 0.05% and with the same size distribution. These results are shown in Fig. 8. A comparison of Figs. 7 and 8 shows that limiting the nuclei slows condensation and induces higher saturation ratios. The effect on $W_l$ is transitory and, beyond $Z \simeq 200$ m, the condensate concentration curve is much the same as in the previous case. However, in the second case, much larger drops are formed reflecting the same quantity of liquid partitioned among much fewer nuclei. The mode radius reaches 0.9 $\mu$ vs 0.2 $\mu$ in the previous case. This change in aerosol size would cause

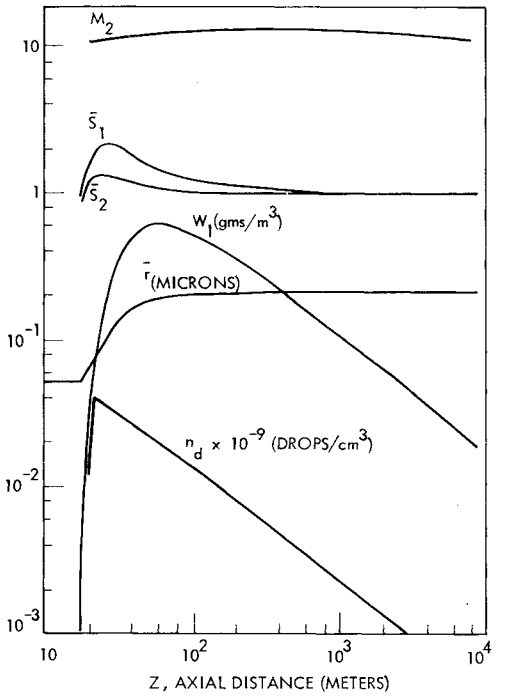


**Fig. 9 Rocket plume condensate aerosol parameters, exhaust nuclei solids mass fraction = 0.05, altitude 14 km.**

significant changes in the optical scattering properties of the contrail.

#### Results at 14 km Altitude

At high altitude, temperatures and saturated vapor pressures are low and, therefore, at a given saturation ratio, condensation is slowed. Thus, limiting the availability of condensation nuclei should have an even greater effect than at lower altitudes. Figures 9 and 10 show two additional sets of calculations similar to the previous examples. Ambient conditions now reflect a 14 km altitude (217 K, 142 mb) and 40% relative humidity. Figure 9 is for an exhaust primary

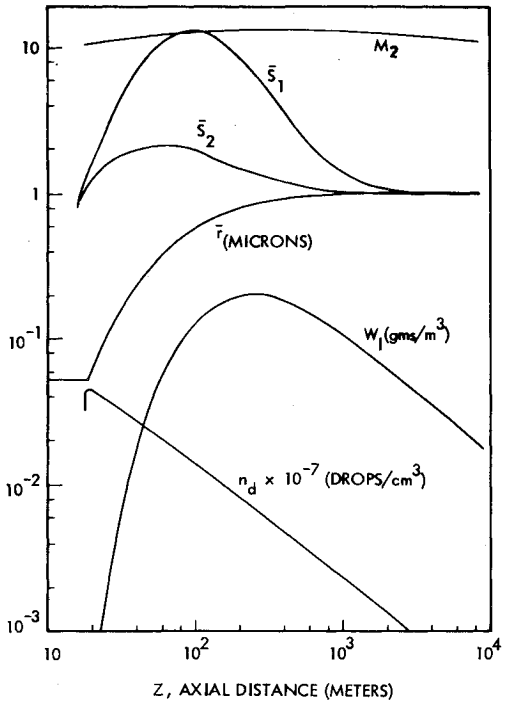


**Fig. 10 Rocket plume condensate aerosol parameters, exhaust nuclei solids mass fraction = 0.0005, altitude 14 km.**

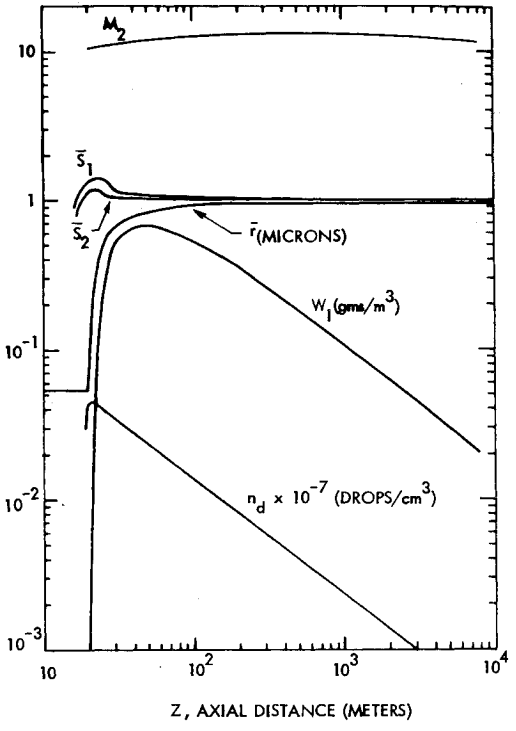


**Fig. 11 Rocket plume condensate aerosol parameters, exhaust nuclei solids mass fraction = 0.05, altitude 7 km, condensation coefficients $\beta_1 = \beta_2 = 1$.**

smoke content of 5% and Fig. 10 shows results with only 0.05% as before.

The comparison of Figs. 9 and 10 show that condensation is now very greatly retarded when the nucleation sites are limited. The maximum plume condensate concentration, $W_l$, is reduced by a factor of 3 in reducing the nuclei content from 5-0.05%. Saturation ratios are also forced to very high levels, e.g., $\bar{S}_1 = 13$. The nuclei density is approximately $1.4 \times 10^5$ cm$^{-3}$ at the point where $\bar{S}_1$ is maximal and this is simply insufficient for condensation to keep up with the formation of supersaturated vapor in the cooling plume. Under these high saturation ratio conditions homogeneous nucleation would become important and the basic model assumption of exclusive heterogeneous nucleation breaks down.

It should be noted that this model limitation is very much a function of the particular primary smoke distribution in use here. The $Al_2O_3$ particle distribution function used to represent the nuclei has a mode diameter of 0.06 $\mu$ and decays rapidly for smaller sizes. There is no reservoir of large numbers of very small particles which would be activated at high saturation ratios. Carbon soot or other materials may play this role in an actual plume. In addition, it is by no means certain that the absence of small particles from the $Al_2O_3$ distribution is real, it may well be due to instrumentation resolution or bias.

### Results with $\beta_1 = \beta_2 = 1$

In order to investigate the sensitivity of results to the condensation coefficient values, two model runs were repeated with the condensation coefficient for water and acid increased from $\beta_1 = \beta_2 = 0.04$ to their maximum possible values of unity. The new result for the 14 km, 0.05% primary smoke case (Fig. 10) is shown in Fig. 11. Comparing Figs. 10 and 11 reveals that the droplet growth is faster and less kinetically limited in the $\beta_1 = \beta_2 = 1$ case, as would be expected. However, in both cases, nearly all the nuclei were activated and the ultimate aerosol mode sizes and number densities are virtually the same beyond about $Z = 300$ m.

A similar rerun of the 7 km, 5% primary smoke case gave somewhat different behavior. The original case (Fig. 7) was not kinetically limited to any degree. The new $\beta_1 = \beta_2 = 1$ results are not shown in a separate figure, but differed from those of Fig. 7 in only two significant respects. These were a mode drop size about twice as large throughout most of the contrail and a commensurately lower droplet number density. This difference arose because the higher droplet growth rates resulted in a collapse of plume supersaturation before it became great enough to activate nuclei smaller than 0.11 $\mu$; these represented only about 6% of those activated in the $\beta_1 = \beta_2 = 0.04$ run.

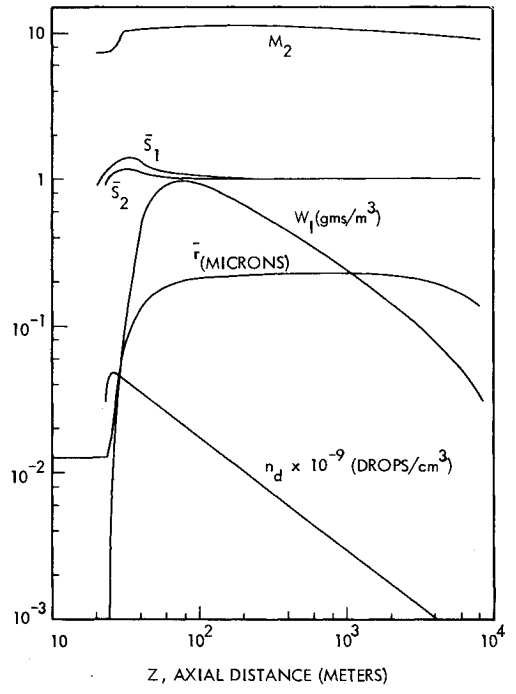


**Fig. 12 Rocket plume condensate aerosol parameters, exhaust nuclei solids mass fraction = 0.0005 (insoluble $Al_2O_3$) + 0.0005 (soluble NaCl) altitude 7 km.**

**Condensation on Soluble Particles**

Changing contrail optical properties by seeding the plume with very large numbers of preferred nucleation sites, thereby decreasing average drop sizes, is an obvious idea. This concept is investigated here by repeating the calculation for the 7 km, 0.05% primary smoke case, this time with additional soluble particles added to the plume. The soluble particles are assumed to be NaCl simply because solution properties data are the most complete for the $NaCl/HCl/H_2O$ system. Based on available solubility data[38] the saturation molality of NaCl in the acid solution is taken to be 5.5. The size distribution parameters are adjusted so that the salt particle mode radius is one-quarter that of the $Al_2O_3$ distribution. Thus, for equal weights, there are then many more NaCl particles than $Al_2O_3$ primary smoke particles. Figure 12 shows the results of the repeat calculation with 0.05% extra NaCl particles added in addition to the 0.05% $Al_2O_3$ particles originally present. Comparing Fig. 12 with the previous results for the $Al_2O_3$ smoke-only case (shown in Fig. 8) reveals that the expected effect is achieved. Namely, that higher drop number densities and concomitant smaller particle sizes are obtained when the fine salt particles are added to the plume.

## Conclusions

A kinetic model has been developed for calculating condensate aerosol properties in rocket contrails. The formulation is based on heterogeneous condensation of the water and acid vapor species on nuclei which are mainly the rocket primary smoke particles. Major conclusions growing out of these studies are as follows:

1) Contrail aerosol drop sizes are strongly dependent on nuclei number densities in the plume. Validating the model by observation of test firings will be difficult until good condensation nuclei size distribution data are available. Firm data on the condensation coefficients for water and acid molecules are also lacking, but quite important.

2) Condensation can be kinetically limited if nuclei are sparse, especially at high altitudes.

3) The droplet growth equations for two-component condensation are stiff and an implicit numerical integration method is necessary.

4) Model calculations show that if the rocket exhaust products contain considerable HCl, the contrail produced generally is a liquid drop aerosol, rather than ice, due to the antifreeze effect of the acid solute.

## Acknowledgment

This work was supported by the Air Force Rocket Propulsion Laboratory under Contract F04611-76-C-0044 and by the Lockheed Independent Research Program.

## References

[1] Hoshizaki, H., Chou, Y. S., Meyer, J. W., Wilson, K. H., Thomas, P.D., "Plume Visibility Detection Study," paper presented at 10th JANNAF Plume Technology Conference, San Diego, Calif., Sept. 1977.

[2] Thomas, P. D. and Wilson, K. H., "Efficient Computation of 'Stiff' Chemically Reacting Flow in Turbulent Free Jets," *AIAA Journal*, Vol. 14, May 1976, pp. 629-636.

[3] Chou, Y. S., "Approximate Method for Radiative Transfer in Scattering Absorbing Plane-Parallel Media," *Applied Optics*, 1977, in press.

[4] Appleman, H., "The Formation of Exhaust Condensation Trails by Jet Aircraft," *Bulletin of the American Meteorological Society*, Vol. 34, Jan. 1953, pp. 14-20.

[5] Jiusto, J. E., "Prediction of Aircraft Condensation Trails," Cornell Aeronautical Lab., Final Rept. VC-1055-P-5 prepared for Office of Naval Research (AD692117), Oct. 1961.

[6] Jiusto, J. E. and Roland, J. P., "Contrails Forecasting," Cornell Aeronautical Lab., Rept. VC-1660-P-3, prepared for Office of Naval Research (AD692119), Aug. 1964.

[7] Oliver, R. C., "Smokeless Solid Propellants: An Overview," Institute for Defense Analyses Res. Paper P-472 (AD502577), March 1969.

[8] Rhein, R. A., "Hydrochloric Acid Aerosol Formation by the Interaction of Hydrogen Chloride with Humid Air," Jet Propulsion Lab., Pasadena, Calif., in 1974 JANNAF Propulsion Meeting, San Diego, Calif., CPIA Publication 260, Dec. 1974, Vol. I, Pt. II, p. 677.

[9] Wegner, P. P. and Stein, G. D., "Light Scattering Experiments and Theory of Homogeneous Nucleation in Condensing Supersonic Flow," *12th Symposium (International) on Combustion*, the Combustion Institute, Pittsburgh, Pa., 1969, pp. 1183-1191.

[10] Howell, W. E., "The Growth of Cloud Drops in Uniformly Cooled Air," *Journal of Meteorology*, Vol. 6, Apr. 1949, pp. 134-149.

[11] Mason, B. J., *The Physics of Clouds*, Clarendon Press, Oxford, England, 1971.

[12] Young, K. C., "A Numerical Simulation of Wintertime, Orographic Precipitation: Part I. Description of Model Microphysics and Numerical Techniques," *Journal of the Atmospheric Sciences*, Vol. 31, Oct. 1974, pp. 1735-1749.

[13] Takahashi, T., "Warm Rain Giant Nuclei and Chemical Balance—A Numerical Model," *Journal of the Atmospheric Sciences*, Vol. 33, Feb. 1976, pp. 269-286.

[14] Clark, T. L., "On Modeling Nucleation and Condensation Theory in the Eulerian Space Domain," *Journal of the Atmospheric Sciences*, Vol. 31, Dec. 1974, pp. 2099-2117.

[15] Miller, E., "The Dynamics of Secondary Smoke Generation in Smokeless Solid Rocket Plumes," paper presented at the 12th International Symposium on Space Science and Technology, Tokyo, May 1977.

[16] Miller, E., "Drop 4: The Modeling of Secondary Smoke in Solid Rocket Plumes," paper presented at the 1977 JANNAF Propulsion Meeting, Incline Village, Feb. 1978.

[17] Miller, E., "The Prediction of Secondary Smoke in Solid Rocket Plumes," paper presented at the 1976 JANNAF Propulsion Meeting, Anaheim, Calif., Dec. 1976.

[18] Miller, E., "The Dynamics of Secondary Smoke Generation in Smokeless Solid Rocket Plumes," paper presented at the 1975 JANNAF Propulsion Meeting, Anaheim, Calif., Oct. 1975.

[19] Victor, A. C., "Computer Codes for Predicting the Formation of Rocket Exhaust Secondary Smoke in Free Jets and Smoke Chambers," Naval Weapons Center Tech. Memo. 3361, Feb. 1978.

[20] Fukuta, N. and Walter, L. A., "Kinetics of Hydrometeor Growth from a Vapor-Spherical Model," *Journal of the Atmospheric Sciences*, Vol. 27, Nov. 1970, pp. 1160-1172.

[21] Fuchs, N. A., *Evaporation and Droplet Growth in Gaseous Media*, Pergamon Press, New York, 1959.

[22] Ranz, W. E. and Marshall, W. R., "Evaporation from Drops," Part II, *Chemical Engineering Progress*, Vol. 48, April 1952, pp. 173-180.

[23] Alty, T. and MacKay, C. A., "The Accommodation Coefficient and the Evaporation Coefficient of Water," *Proceedings of Royal Society*, Series A 149, 1935, pp. 104-116.

[24] Mills, A. F. and Seban, R. A., "The Condensation Coefficient of Water," *International Journal of Heat and Mass Transfer*, Vol. 10, 1967, pp. 1815-1827.

[25] Hamer, W. J. and Wu, Y. C., "Osmotic Coefficients and Mean Activity Coefficients of Uniunivalent Electrolytes in Water at 25°C," *Journal of Physical Chemistry Reference Data*, Vol. 1, 1972, pp. 1047-1097.

[26] Robinson, R. A. and Stokes, R. H., "Tables of Osmotic and Activity Coefficients of Electrolytes in Aqueous Solution at 25°C," *Transactions of Faraday Society*, Vol. 45, 1949, pp. 612-624.

[27] Stokes, R. H., "A Thermodynamic Study of Bivalent Metal Halides in Aqueous Solution. Part XVII-Revision of Data for All 2:1 and 1:2 Electrolytes at 25°, and Discussion of Results," *Transactions of Faraday Society*, Vol. 44, 1948, pp. 295-307.

[28] Harned, H. S. and Owen, B. B., *The Physical Chemistry of Electrolytic Solutions*, R. Reinhold, New York, 1958.

[29] Akerlof, G. and Teare, J. W., "Thermodynamics of Concentrated Aqueous Solutions of Hydrochloric Acid," *Journal of the American Chemical Society*, Vol. 55, Oct. 1937, pp. 1855-1868.

[30] Harned, H. S. and Gary, R., "The Activity Coefficient of Hydrochloric Acid in Concentrated Aqueous Higher Valence Type Chloride Solutions at 25°I the System Hydrochloric Acid-Barium Chloride," *Journal of the American Chemical Society*, Vol. 76, Dec. 1954, pp. 5924-5927.

[31] Harned, H. S., "The Thermodynamic Properties of the System: Hydrochloric Acid, Sodium Chloride, and Water from 0 to 50°," *Journal of Physical Chemistry*, Vol. 63, Aug. 1959, pp. 1299-1302.

[32] Leyendekkers, J. V., "Activity Coefficients in Mixed Solutions, Prediction of Harned Coefficients from Ionic Entropies," *Journal of Physical Chemistry*, Vol. 74, May 1970, pp. 2225-2229.

[33] Harned, H. S. and Gary, R., "The Activity Coefficient of Hydrochloric Acid in Concentrated Aqueous Higher Valence Type Chloride Solutions at 25°. III. The System Hydrochloric Acid-Aluminum Chloride," *Journal of the American Chemical Society*, Vol. 77, Sept. 1955, pp. 4695-4697.

[34] Storonkin, A. V., Lagunov, M. D., and Prokoteva, R. V., "Aqueous Solutions of Strong Electrolytes. II. Activity of Hydrochloric Acid in the Systems HCl-$MgCl_2$-$H_2O$, HCl, $CaCl_2$-$H_2O$, HCl-Sr $Cl_2$-$H_2O$, and HCl-A $Cl_3$-$H_2O$," *Russian Journal of Physical Chemistry*, Vol. 39, Aug. 1965, pp. 1070-1072.

[35] Perry, J. H., ed., *Chemical Engineers Handbook*, 3rd ed., McGraw-Hill, New York, 1950, p. 167.

[36] Dawbarn, R. and Kinslow, M., "Studies of the Exhaust Products from Solid Propellant Rocket Motors," Arnold Air Force Station, Tenn., AEDC-TR-76-49, Sept. 1976.

[37] Dawbarn, R., ARO, Inc. Arnold Air Force Station, Tenn., private communication, 1976.

[38] Linke, W. F., *Solubilities Vol. II*, D. Van Nostrand, 1958, pp. 962-963.